Supplemental Material

Supplemental Figures

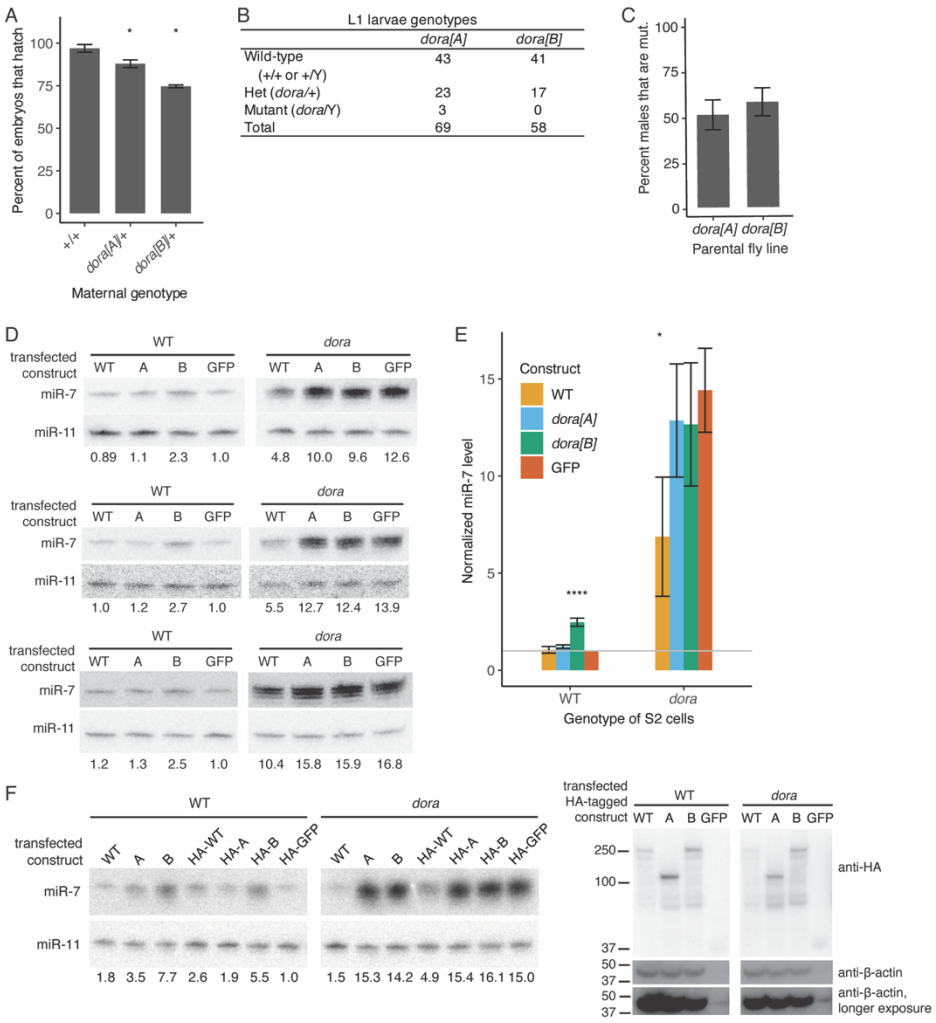

Figure S1. Characterization of *dora[A]* and *dora[B]* Alleles, related to Figure 1
(A) Hatching frequencies of embryos from *dora* crosses using mothers that lacked a balancer. Either wild-type (+/+) or *dora* heterozygous (*dora*/+) mothers were crossed with wild-type (+/Y) fathers. Error bars indicate standard error (n = 2 sets of 300 embryos for +/+ crosses, and 4 sets of 300 embryos for *dora*/+ crosses), and asterisks denote significance relative to the +/+ crosses determined with a t-test (*, $p <$ 0.05). Hatching frequencies of embryos produced from crosses with *dora*/+ mothers were increased relative to hatching frequencies observed from mothers carrying the FM7c balancer (Figure 1B) (from 81% to 88% and from almost 50% to 75% for the *dora[A]* and *dora[B]* crosses, respectively), suggesting that synthetic lethality with FM7c occurs with both *dora* alleles. Confirming that the FM7c balancer does not promote substantial embryonic lethality on its own, control crosses carried out with mothers heterozygous for FM7c and fathers hemizygous for FM7c had hatching frequencies >95% (Figure 1B).
(B) Genotyping results for early L1 larvae produced from *dora* crosses using mothers that lacked a balancer (as in A). Otherwise, this panel is as in Figure 1C.
(C) Rescue of lethality with an X-chromosomal duplication that is located on the third chromosome and contains the *Dora* locus (Dp(1;3)DC353). Females that were heterozygous for either the *dora[A]* or the *dora[B]* allele were crossed to males homozygous for the duplication, and male progeny were genotyped

to assess the fraction that carried a *dora* allele. Error bars indicate standard deviation (*n* = 2 independent crosses for both genotypes).
(D) The ability of *Dora* variants to rescue TDMD in S2 cells mutant for Dora (*dora*). Either wild-type or *dora* S2 cell lines were transfected with a construct expressing either wild-type *Dora* (WT), *dora[A]* (A), *dora[B]* (B), or GFP, and total RNA was analyzed on blots probed for miR-7 (a TDMD substrate) and miR-11 (a loading control). Each panel corresponds to an individual blot reporting the results for a unique pair of clonal wild-type (WT) and *dora* S2 cell lines (Shi et al., 2020). Signals for miR-7 were each normalized to that of the loading control, and numbers below each blot show miR-7 levels relative to that observed for GFP-transfected wild-type cells. Superfluous lanes were cropped from the blot, as denoted by the vertical spaces.
(E) Summary of the results from (D). Error bars show the standard deviation (*n* = 3), and asterisks denote significant differences relative to transfection of the wild-type construct (wild-type cells) or transfection of the GFP construct (*dora* cells), evaluated with ANOVA and the Tukey test (*, $p < 0.05$; ****, $p < 0.0001$).
(F) Additional replicates of the rescue experiment of (D), performed with HA-tagged *Dora* variants in addition to untagged variants used in (D). The Northern blot (left) is as in (D), with expression of the HA-tagged variants shown on the accompanying western blot (right). For the western blot, samples from cells expressing HA-GFP were diluted 1:50 prior to loading to account for the stronger signal detected for these samples due to greater accumulation and presumably more efficient transfer of the lower-molecular-weight protein. β-actin is used as a loading control; a shorter exposure is shown for comparing bands in the lanes with HA-tagged Dora variants, and a longer exposure is shown to enable visualization of bands in the lanes with HA-GFP.

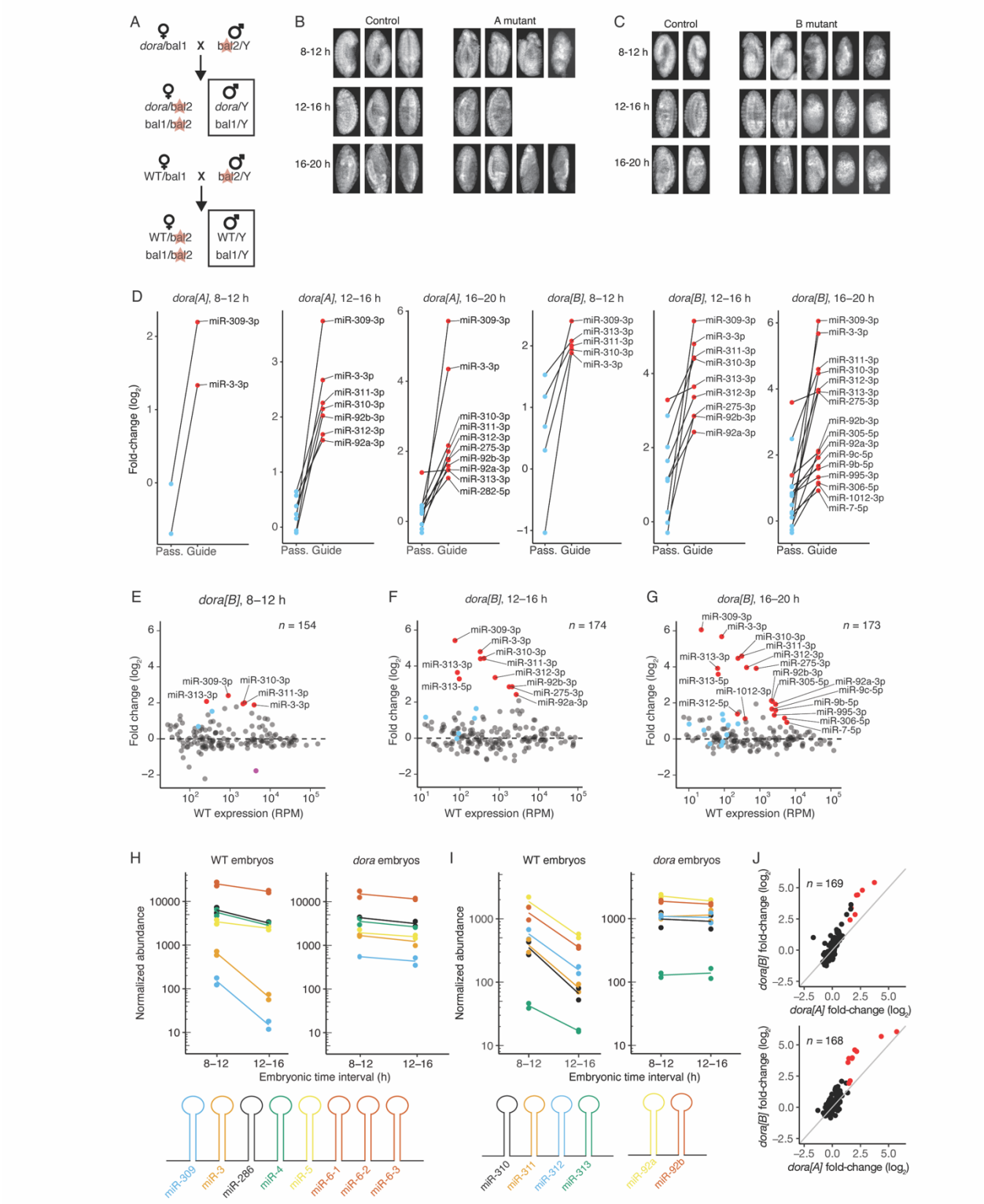

Figure S2. miRNA Dysregulation in *dora* Embryos, related to Figure 1

(A) Scheme of cross used to isolate a population of embryos enriched for the *dora* allele. Bal1 and bal2 are X-chromosome balancers FM7c and FM7a, respectively, and bal2 expresses RFP ubiquitously under the *sqh* promoter (red star). Sorting for embryos without red fluorescence yielded of a pool of male embryos, of which either 50% or 0% were mutant at the *dora* locus (left and right crosses, respectively).

(B and C) Images of DAPI-stained RFP-negative embryos from wild-type (control) and *dora[A]* (B) or *dora[B]* (C) crosses, acquired at the indicated time intervals. Although many embryos from the *dora[B]* cross were misformed (C), only a single misformed embryo was observed in the set of sorted embryos acquired from the *dora[A]*cross (B, 8-12 h cohort).
(D) Fold-changes observed for Dora-sensitive guide strands and their passenger-strand partners in embryos from the *dora[A]* (left three panels) and *dora[B]* (right three panels) crosses. Guide strands were each annotated as the strand from the miRNA duplex that was more abundant in *dora* samples. Changes were determined by DEseq analyses of sRNA-seq data, with each genotype represented by two replicates at each time interval. In contrast to the data shown in Figure 1D–F and Figure S2E–G, the default DEseq filtering was used (Love et al., 2014), without application of an additional, more stringent expression cutoff; this more permissive DEseq filtering enabled visualization of more passenger/guide pairs. Points are colored as in Figure 1D–F and Figure S2E–G. Thus, in three samples both miR-313-3p and its passenger strand (miR-313-5p) were considered Dora-sensitive, and in one sample both miR-312-3p and its passenger strand (miR-312-5p) were considered Dora-sensitive. Note that although the 5p and 3p strands of miR-313 were each typically upregulated to a similar degree, passenger strands of other miRNAs co-transcribed from this cluster (e.g., miR-311-5p and miR-312-5p) were not upregulated to a similar degree as their guide strands, implying that both miR-313-3p and miR-313-5p are Dora sensitive.
(E–G) As in Figure 1D–F, but for the *dora[B]* 8–12 h (E), 12–16 h (F), and 16–20 h (G) samples.
(H) As in Figure 1G, but for *dora[B]*.
(I) As in Figure 1H, but for *dora[B]*.
(J) Correlation of fold-changes observed upon loss of Dora in *dora[A]* and *dora[B]* samples for the 12–16 h (top) and 16–20 h (bottom) time intervals. Points colored in red were called as significant in both the *dora[A]* and *dora[B]* samples.

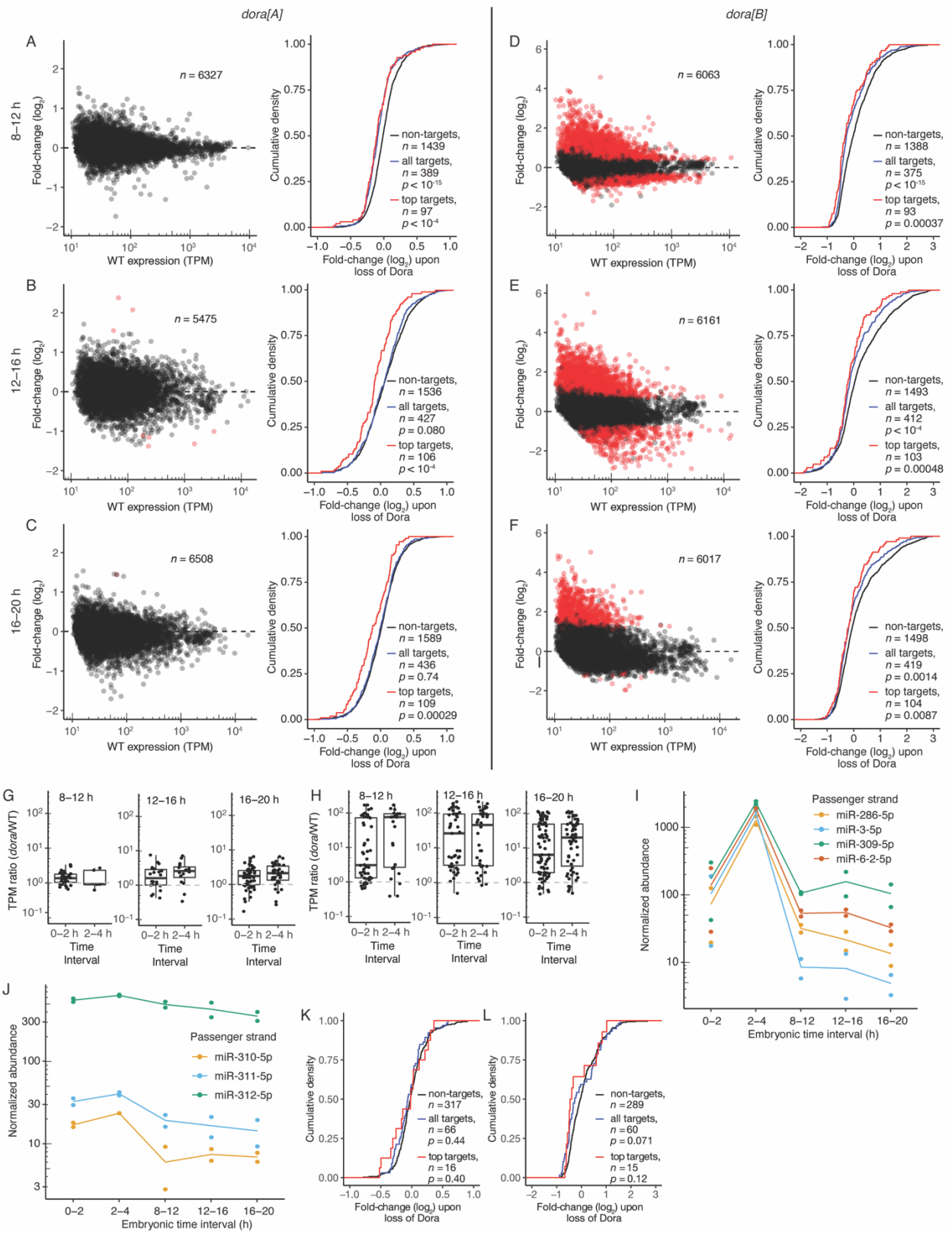

Figure S3. mRNA Dysregulation upon Loss of Dora, related to Figure 1

(A) mRNA changes observed upon loss of Dora in 8–12 h embryos. The left panel shows mean fold-changes as a function of WT expression, as determined by DEseq, with red (when present) indicating mRNAs with significant changes (DEseq-adjusted $p < 0.05$). The right panel shows cumulative distributions of these fold-changes for conserved predicted targets (blue) and top predicted targets (red) of the miR-310 family, and for a representative cohort of mRNAs not predicted to be targets but with a distribution of 3′ UTR lengths matching that of the predicted targets (non-targets, black). *p* values each indicate the significance of the difference between the distribution and the non-target distribution, evaluated using the two-sided Kolmogorov-Smimov test.
(B and C) As in (A) but for 12–16 h (B), and 16–20 h (C) *dora[A]* samples.
(D and F) As in (A–C) but for *dora[B]* samples.
(G and H) Evidence for inclusion of developmentally arrested embryos. Plotted are the ratios of mRNA abundances (in TPM) for a set of genes used to diagnose contamination with embryos stalled early in development for *dora[A]* (G) or *dora[B]* (H) embryos. The striking dysregulation observed in the *dora[B]* samples led to concern that the presence of developmentally arrested embryos might have obscured the true dysregulation occurring after of loss of Dora. To evaluate this possibility, we examined whether mRNAs more highly expressed early in embryonic development were more abundant in embryos from the *dora* crosses than in embryos from wild-type crosses. For each time interval, these analyses indicated the presence of material from embryos stalled early during embryogenesis, although the inferred amount of this early embryonic material was much greater for *dora[B]* time intervals than for *dora[A]* time intervals.
(I and J) Abundance of representative passenger strands from the *mir-3* cluster (I) or *mir-310* cluster (J) in wild-type embryos across embryogenesis. Data were from sRNA-seq of wild-type control embryos generated in parallel with the *CR43432* embryos. Points show results of replicates for each timepoint, after normalizing to quantitative internal standards, and the solid line connects the average of these values. These data, together with the sRNA-seq data from *dora[A]* or *dora[B]* embryos (Table S1B) were used to assess potential contamination by arrested embryos as follows: First, we note that the analyses presented in (G–H) were limited by the lack of quantitative standards in RNA-seq samples, which complicated determination of the degree of contamination from arrested embryos, as changes in total RNA levels could not be accounted for. Therefore, we analyzed sRNA-seq libraries, for which we did have quantitative standards, assessing the levels of miRNA passenger strands whose expression peaked early in embryonic development. As the passenger-strand levels for the *mir-3* cluster were approximately equal at the 0–2, 8–12, 12–16, and 16–20 h time intervals (I), only contamination with 2–4 h embryos would have led to inflated expression of this cluster in *dora* samples. We did not observe inflated levels of these passenger strands in either the *dora[A]* or *dora[B]* embryos (Table S1B), implying that any contamination was predominantly with embryos arrested at an earlier stage, i.e., 0–2 h. Passenger-strand levels for the *mir-310* cluster were higher at 0–2 h compared to 8–12 h and later (J), and thus could speak to the degree to which *dora* samples were contaminated by 0–2 h embryos. We did not observe strikingly inflated levels for of passenger strands of the *mir-310* cluster in *dora[A]* samples (Table S1B), which confirmed the conclusions from the RNA-seq analyses (G). However, we did observe increased levels of the passenger strands from the *mir-310* cluster in the *dora[B]* samples (Figures S2D–G; Table S1B), which indicated larger amounts of contamination in these samples. Although these analyses provided more information about the lethal nature of the *dora[B]* allele, indicating that some embryos from the *dora[B]* cross were arrested or died very early, they also prevented any strong conclusions from being drawn from *dora[B]* RNA-seq samples regarding the primary effects of disrupting TDMD on gene expression.
(K and L) As in the right panel in (A), but for predicted targets of the miR-3 family in 8–12 h *dora[A]* (K) and *dora[B]* (L) samples.

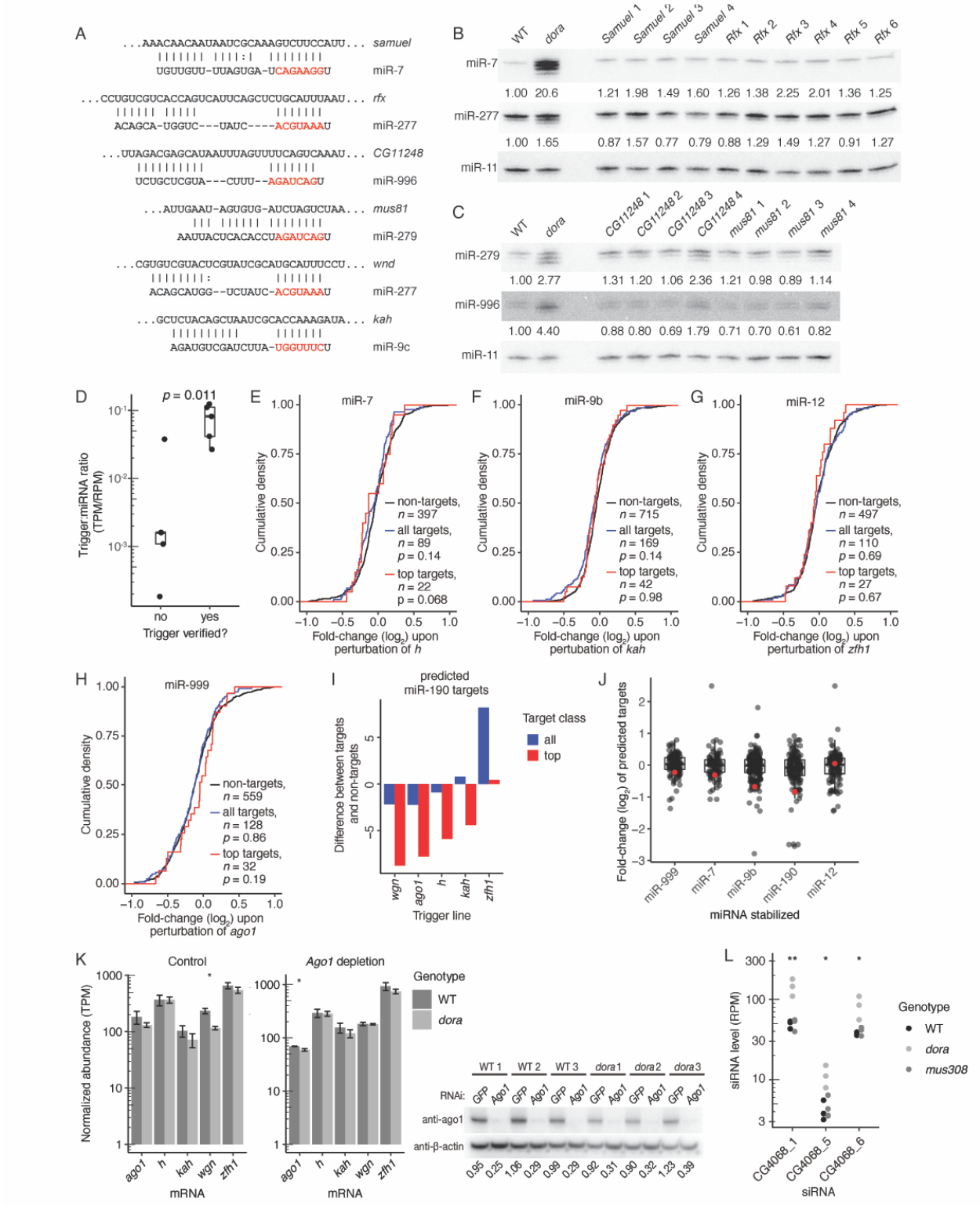

Figure S4. Validation and Evaluation of Candidate TDMD Trigger Sites, related to Figures 2 and 3

(A) Pairing diagrams for candidate trigger sites that failed to validate in S2 cells. Otherwise, this panel is as in Figure 2A.

(B and C) Results of experiments that failed to validate candidate trigger sites in S2 cells. Northern blots were probed for miR-7, miR-277, miR-279, and miR-996 following disruption of their candidate trigger

sites in the genes *Samuel*, *Rfx*, *mus81*, and *CG11248*, respectively. Otherwise, this panel is as in Figure 2B–C.
(D) Distributions of trigger:miRNA ratios for candidate trigger sites that either validated or failed to validate in S2 cells. Each trigger:miRNA ratio was calculated by dividing the average TPM of the trigger in wild-type S2 cells by the average RPM of the miRNA in *dora* S2 cells.
(E–H) As in Figure 3A, but for miR-7 predicted targets upon disruption of *h* (E), miR-9b predicted targets upon disruption of *kah* (F), miR-12 predicted targets upon disruption of *zfh1* (G), and miR-999 predicted targets upon disruption of *ago1* (H).
(I) Analyses questioning the specificity of the changes in miR-190 predicted targets observed upon perturbation of the trigger site in *wgn*. Plotted are relative differences in fold-change distributions observed for the two classes of miR-190 predicted targets as compared to the non-target distribution upon perturbation of each trigger site identified in S2 cells. The relative difference between the distributions was estimated as the cumulative difference of fold-change values of target and the non-target cumulative-distribution curves at each integer percentile from 5% to 95%, with negative values indicating greater repression for the target class examined. Sets of predicted targets were as in Figure 3A. Perturbation of the trigger site in *wgn* stabilized miR-190, whereas none of the other trigger sites were predicted to regulate miR-190 levels.
(J) Fold-changes observed upon loss of Dora for conserved predicted targets of each of the five miRNAs for which a trigger was identified in Drosophila S2 cells. Colored in red is the TDMD trigger identified for each miRNA.
(K) The effect of Ago1 on reduced trigger levels observed upon loss of Dora. The panels at the left and center are is as in Figure 3C, but for either control samples (*GFP* RNAi, left panel), or *Ago1*-depleted samples (center panel). The panel on the right is a western blot showing successful depletion of Ago1 following treatment of either wild-type or *dora* clonal S2 cell lines with RNAi, with β-actin acting as a loading control. Quantification of normalized Ago1 abundance is shown below each lane of the western blot; values are relative to the average Ago1 abundance in wild-type (*GFP* RNAi) samples.
(L) Evidence that target slicing can dominate over target-directed siRNA degradation. Plotted are abundances of three siRNAs associated with Ago1 in wild-type, *dora*, or *mus308* S2 cells, with each point representing results from a unique clonal cell line (Table S3) (Shi et al., 2020). Drosophila S2 cells express small-interfering RNAs (siRNAs) in addition to miRNAs, and some of these endogenous siRNAs are Dora-sensitive when loaded into Ago1 (Kingston and Bartel, 2021). Endogenous siRNAs can direct target slicing, which requires a highly complementary site (Okamura et al., 2004; Förstemann et al., 2007). Exogenous expression of such slicing-competent sites can trigger degradation of miRNAs in Drosophila S2 cells, promoting between 2- and 5-fold decreases in miRNA abundance (Ameres et al., 2010). As a highly complementary, slicing-competent site in the mRNA *mus308* has been identified for three of the Dora-sensitive siRNAs (siRNAs CG4068_1, CG4068_5, CG4068_6) (Czech et al., 2008; Okamura et al., 2008), we postulated that perhaps this site might direct degradation of these siRNAs. To test this idea, we used Cas9 to disrupt the site in *mus308*, and measured Ago1-loaded CG4068_1, CG4068_5, and CG4068_6 levels in wild-type, *dora*, and *mus308* cells. Although the Ago1-loaded population of these siRNAs was upregulated upon loss of Dora (*, $p < 0.05$; **, $p < 0.01$; ANOVA and the Tukey test), disruption of the site in *mus308* did not significantly alter the levels of these siRNAs. Thus, these siRNAs were able to direct slicing of this site, yet this site was not able to direct degradation of these siRNAs. These results support a model in which extensively paired sites capable of being sliced are not efficient triggers of target-directed degradation because slicing destroys the sites before the TDMD machinery can act (Sheu-Gruttadauria et al., 2019).

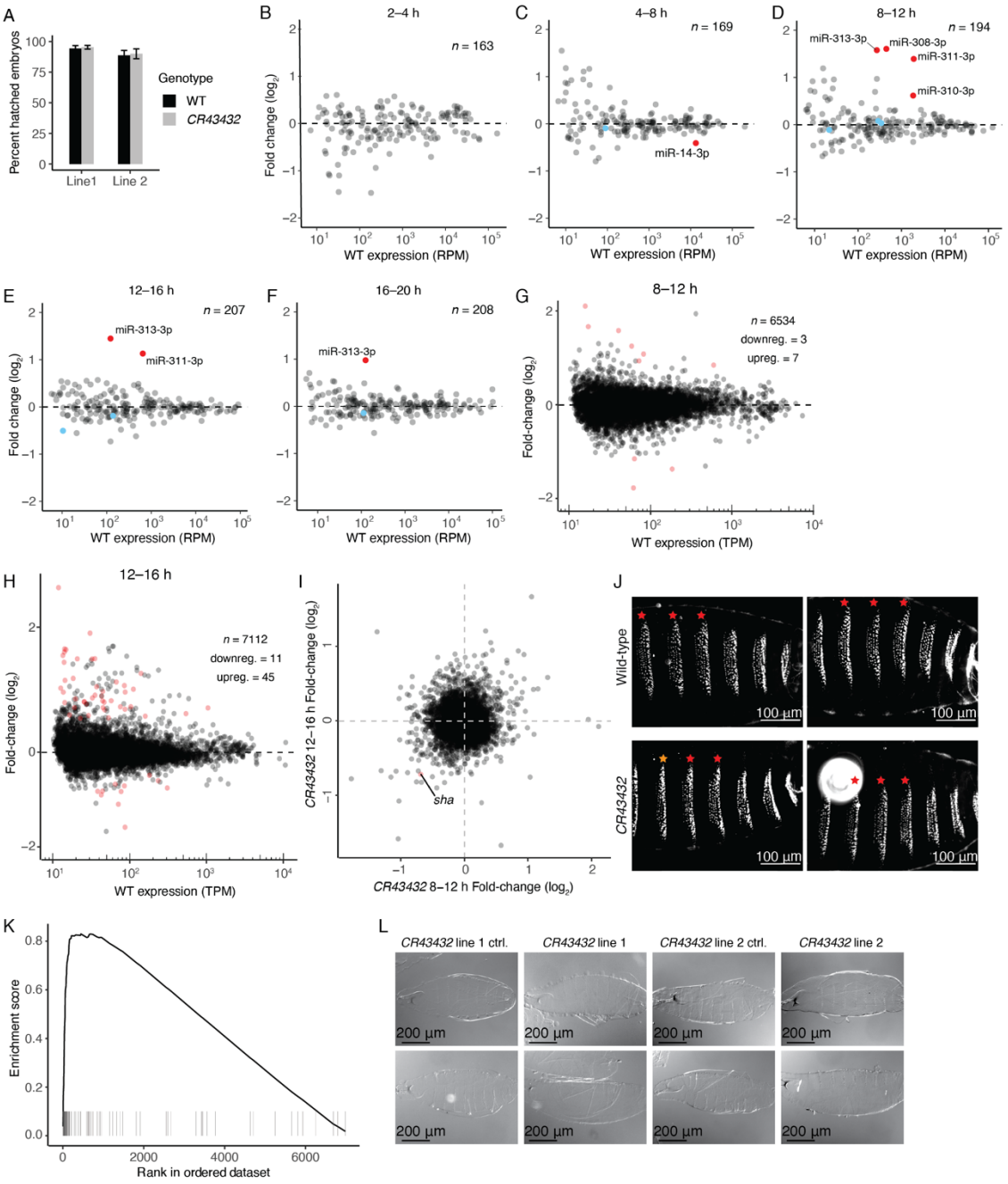

Figure S5. CR43432 Directs Degradation of Select miR-310 Family Members, which Promotes Proper Cuticle Development, related to Figure 4

(A) Hatching frequency of embryos produced from crosses of either wild-type (black) or *CR43432* (grey) flies. Error bars indicate standard error (n = 3 sets of 100 embryos for each genotype); the difference in hatching frequencies between the wild-type and *CR43432* flies for both lines is not significant (as evaluated by a *t*-test).

(B–F) Changes in miRNA levels observed upon perturbation of the miR-310 family site in CR43432, as determined by sRNA-seq. Shown are results for 2–4 h (B), 4–8 h (C), 8–12 h (D), 12–16 h (E), and 16–20 h (F) embryos, with each point representing the mean from the two biological replicates (each with independently derived lines, Table S3), as determined by DEseq. Shown in red and labeled are miRNAs with significantly different levels (adjusted $p < 0.05$) in *CR43432* embryos.

(G and H) Changes in mRNA levels observed upon disruption of the site for the miR-310 family in *CR43432*, as determined by mRNA-seq. Shown are results for 8–12 h (G) and 12–16 h (H) embryos, with each point representing the mean from two biological replicates (each with independently derived lines, Table S3), as determined by DEseq. Red points indicate mRNAs that were significantly up or down-regulated (adjusted $p < 0.05$).
(I) Comparison of mRNA fold-changes in *CR43432* 8–12 and 12–16 h embryos, as quantified in panels (G) and (H). In red and labeled is the point for *shavenoid*.
(J) Representative dark-field images of cuticles of wild-type and *CR43432* late-stage embryos. Embryos are oriented with posterior to the right, and the stars denote the fourth, fifth, and sixth denticle belts. Red stars indicate belts quantified for the analyses in Figure 4F, and orange stars indicate belts not quantified due to distortion.
(K) GSE analysis for the gene set 'chitin-based cuticle development.' Genes are ranked according to DEseq-determined mean fold-changes observed upon disruption of the site in *CR43432*, with lower ranks corresponding to the most strongly up-regulated genes.
(L) Representative bright-field images of mechanically devitellinized cuticles for wild-type (line 1 ctrl and line 2 ctrl) or *CR43432* (line 1 or line 2) late-stage embryos. All cuticles are oriented with the anterior to the left.